ACS APPLIED MATERIALS & INTERFACES

Research Article

www.acsami.org

Origin of Outstanding Phase and Moisture Stability in a $Na_3P_{1-x}As_xS_4$ Superionic Conductor

Shun-Li Shang,*[,†] Zhaoxin Yu,[‡] Yi Wang,[†] Donghai Wang,[‡] and Zi-Kui Liu[†]

[†]Department of Materials Science and Engineering and [‡]Department of Mechanical and Nuclear Engineering, The Pennsylvania State University, University Park, Pennsylvania 16802, United States

Supporting Information

ABSTRACT: Sodium ion (Na) solid-state electrolytes (SSEs) are critical to address notorious safety issues associated with liquid electrolytes used in the current Na ion batteries. Fulfilling multiple innovations is a grand challenge but is imperative for advanced Na ion SSEs, such as a combination of high ionic conductivity and excellent chemical stability. Here, our first-principles and phonon calculations reveal that $Na_3P_{1-x}As_xS_4$ ($0 \le x \le 1$) is a solid-state superionic conductor stabilized at 0 K by zero-point vibrational energy and at finite temperatures by vibrational and configurational entropies. Especially, our integrated first-principles and experimental approach indicates that $Na_3P_{1-x}As_xS_4$ is dry-air stable. Additionally, the alloying element arsenic greatly enhances the moisture (i.e., H_2O) stability of $Na_3P_{1-x}As_xS_4$ by shifting the reaction products from the easy-forming oxysulfides (such as Na_3POS_3 and $Na_3PO_2S_2$ with H_2S release) to the difficult-forming hydrates (such as $Na_3P_{1-x}As_xS_4{\cdot}nH_2O$ with n = 8 and/or 9) due mainly to a weaker As−O affinity compared to that of P−O. The present work demonstrates that alloying is able to achieve multiple innovations for solid-state electrolytes, such as a desirable superionic conductor with not only a high ionic conductivity (for example, 1.46 mS/cm at room temperature achieved in $Na_3P_{0.62}As_{0.38}S_4$) but also an excellent chemical stability with respect to temperature, composition, and moisture.

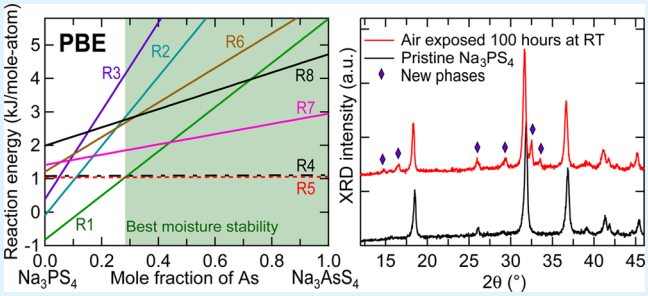

KEYWORDS: *Na ion solid-state electrolytes, $Na_3P_{1-x}As_xS_4$, phase stability, moisture stability, first-principles and phonon calculations, X-ray diffraction*

1. INTRODUCTION

Rechargeable Na ion batteries present a promising low-cost, sustainable alternative to today's Li ion batteries for use in medium- and large-scale energy storage systems because of the abundant sodium resources and the dwindling lithium supplies.[1−3] However, current Na ion batteries still suffer from notorious safety issues due mainly to the volatile and flammable liquid electrolyte and the high reactivity of Na metal deposited upon overcharging. This hence promotes the development of solid-state electrolytes (SSEs) which would make the all-solid-state Na ion batteries much safer and resistant to leakage and would achieve a long cycle life, and thereby would accelerate their deployment in critical energy technologies where safety is a major concern.[4,5]

Among the developed SSEs, sulfides were found superior to oxides to achieve high ionic conductivity and hence more suitable for all-solid-state batteries,[6,7] for example, the breakthrough discovery of $Li_{10}GeP_2S_{12}$ (LGPS)[8] with a room temperature (RT) conductivity σ_{RT} = 12 mS/cm and the finding of LGPS-type $Li_{9.5}Si_{1.74}P_{1.44}S_{11.7}Cl_{0.3}$ with a record-breaking σ_{RT} = 25.3 mS/cm.[9] Inspired by the success in LGPS-type SSEs, considerable Na ion chalcogenide conductors with encouraging σ_{RT} values have been developed and are summarized in Table 1,[7,10−16] where the initial finding is a glass-ceramic Na_3PS_4 by Hayashi et al.[10] with σ_{RT} = 0.2−0.46 mS/cm.[10−12] The subsequent findings from experiments include the Na_3PS_4-type Na_3PSe_4, Na_3AsS_4, Na_3SbS_4, $Na_{2.9375}PS_{3.9375}Cl_{0.0625}$, and $Na_3P_{0.62}As_{0.38}S_4$ as well as the LGPS-type $Na_{10}SnP_2S_{12}$ and $94Na_3PS_4{\cdot}6Na_4SiS_4$ (see their σ_{RT} values in Table 1). In addition, first-principles calculations by Zhu et al.[17] indicated that a higher Si doping such as x_{Si} = 0.125 could yield

Table 1. Measured Na Ion Conductivities at Room Remperature (σ_{RT}, mS/cm) for Na Ion SSEs

Na ion SSE	σ_{RT}	note
Na_3PS_4	0.2−0.46	our previous work and refs 10−12
Na_3AsS_4	0.027	our previous work[12]
Na_3SbS_4	1.10	ref 7
Na_3PSe_4	1.16	ref 13
$Na_3P_{0.62}As_{0.38}S_4$	1.46	our previous work[12]
$Na_{2.9375}PS_{3.9375}Cl_{0.0625}$	1.14	ref 14
$94Na_3PS_4{\cdot}6Na_4SiS_4$	0.74	ref 15
$Na_{10}SnP_2S_{12}$	0.4	ref 16

Received: March 13, 2017
Accepted: April 28, 2017
Published: April 28, 2017

DOI: 10.1021/acsami.7b03606
ACS Appl. Mater. Interfaces 2017, 9, 16261−16269

a significant increase of Na ion conductivity in Na_3PS_4. Here, special attention should be paid to the most promising $Na_3P_{0.62}As_{0.38}S_4$—our recent experimental finding with the highest σ_{RT} = 1.46 mS/cm reported so far in sulfide SSEs[12]—indicating the vital role of the alloying element arsenic to enhance Na ion conductivity in Na_3PS_4 (also true in the Li ion case as demonstrated in $Li_{3.833}Sn_{0.833}As_{0.166}S_4$).[6]

In addition to the challenge in developing Na ion SSEs with high conductivity that are comparable with liquid counterparts (around 6−8 mS/cm at room temperature),[18] chemistry stability is another challenge especially for phosphorus−sulfur-based electrolytes with inferior stability in air and moisture compared to oxides (for example, $Li_{10}GeP_2S_{12}$ and Na_3PS_4).[6,7] This challenge imposes a serious environmental concern and makes their broad application questionable. Furthermore, the sensitivity of SSEs in air and moisture necessitates sophisticated and complex treatment procedures under a dry inert gas atmosphere, which increases their processing cost.[6,19] For the present focus of $Na_3P_{1-x}As_xS_4$, it is dry-air stable against oxygen but moisture unstable with respect to H_2O, especially when the arsenic mole fraction $x < \sim 0.25$ (see details later). Moisture instability of sulfides (using Na_3PS_4 as an example) can be understood by the negative reaction Gibbs energy (ΔG_r) in the following reactions (separately or in combination):

$$S^{2-} + H_2O \rightarrow O^{2-} + H_2S \quad (1)$$

$$Na_3PS_4 + nH_2O \rightarrow Na_3PS_4{\cdot}nH_2O \quad (2)$$

Besides air and especially moisture stability, phase stability with respect to temperature and alloying elements is another concern about stability, which determines the application range of SSEs.

As an effort to explore the promising superionic conductor $Na_3P_{0.62}As_{0.38}S_4$ (see its σ_{RT} value in Table 1),[12] the present work aims to identify the role of the alloying element arsenic in regulating the stability of $Na_3P_{1-x}As_xS_4$ with respect to temperature, composition, air, and moisture (mainly H_2O). To this end, an integrated approach is employed in the present work including density functional theory (DFT)-based first-principles and phonon calculations together with experimental synthesis and characterization. Besides the increased Na ion conductivity due to the alloying element arsenic,[12] here, we reveal that $Na_3P_{1-x}As_xS_4$ is stable at 0 K due to the zero-point vibrational energy, and it possesses enhanced moisture stability stemming from a weaker As−O bonding with respect to the P−O bonding. Hence, the reaction products of "$Na_3P_{1-x}As_xS_4 + H_2O$" shift from the easy-forming oxysulfides to the difficult-forming hydrates with increasing arsenic content.

2. EXPERIMENTAL AND COMPUTATIONAL METHODS

2.1. Materials Synthesis and Characterization. *2.1.1. Synthesis.* As detailed previously,[12] solid-state electrolyte $Na_3P_{1-x}As_xS_4$ ($0 \le x \le 1$) was synthesized by the ball-mill technique followed by heat treatment in terms of Na_2S (Alfa Aesar, anhydrous, analytical reagent), P_2S_5 (Sigma-Aldrich, 99%), and As_2S_5 (Sigma-Aldrich, 99.99%). A mixture of these precursors was ball-milled for 15 h at a speed of 510 rpm using the planetary ball mill (Across International). The obtained powder samples were cold pressed at 400 MPa into a pellet 10 mm in diameter and 0.6−1.2 mm in thickness. All these processes were protected under an argon atmosphere due to the possible air and moisture instability of $Na_3P_{1-x}As_xS_4$. The prepared pellets were sealed in an evacuated glass tube and heated to 270 °C at a rate of 1 °C/min, and then kept at 270 °C for 2 h before being cooled to room temperature at the same rate.

2.1.2. Characterization. Power X-ray diffraction (XRD) was performed on a Rigaku Miniflex II spectrometer with Cu Kα radiation. A beryllium window (Rigaku Corp.) was used as the XRD holder for atmosphere-sensitive samples. The samples were sealed with Kapton tape in a glovebox filled with high-purity argon gas to avoid any side reactions with air (mainly oxygen) and moisture (mainly H_2O). The morphology of these pellets was characterized with a scanning electron microscope (Nano630 FE-SEM). The mole fraction of arsenic in $Na_3P_{1-x}As_xS_4$ was determined by inductively coupled plasma emission spectrometry (ICP-AES; PerkinElmer Optima 5300).

2.2. Structure Consideration and Possible Reaction Products. According to XRD and synchrotron XRD patterns and DFT calculations,[12] Na_3PS_4 as well as $Na_3P_{1-x}As_xS_4$ can be described well by a tetragonal phase with space group $P\bar{4}2_1c$ due mainly to the (212) diffraction peak;[20] see also the present XRD patterns shown later. In addition to the low-energy tetragonal phase, the perfect cubic phase (Wyckoff site 6b in space group $I\bar{4}3m$ fully occupied by Na) and the defect cubic phase (Wyckoff sites 6b and 12d in space group $I\bar{4}3m$ partially occupied by Na)[21] were also tested for $Na_3P_{1-x}As_xS_4$ in the present work, since they are widely used in the literature.[10,21] To account for the variation of arsenic concentration in $Na_3P_{1-x}As_xS_4$, a 128-atom supercell was employed in terms of space group $P\bar{4}2_1c$. All the independent $Na_{48}(P_{1-x}As_x)_{16}S_{64}$ structures were generated by the ATAT code.[22] Special attention was paid to composition $Na_3P_{0.5}As_{0.5}S_4$: (i) a low-energy structure with space group $P2_1$ including 32 atoms in the primitive cell and (ii) a high-energy structure with space group $P\bar{4}$ including 16 atoms in the primitive cell. More details about the $Na_3P_{1-x}As_xS_4$ structures are given in Table S1 of the Supporting Information as well as our previous paper.[12]

The possible reaction products from "$Na_3P_{1-x}As_xS_4 + H_2O$", see eqs 1 and 2, were examined by "Structure Predictor" in the Materials Project[23−25] using the data-mined knowledge of experimental crystal data, i.e., the ICSD (Inorganic Crystal Structure Database).[26] Note that some possible reaction products were excluded in the present work due to the lack of atomic positions for first-principles calculations, for example, $Na_3AsO_3S{\cdot}12H_2O$ with unknown hydrogen positions[27] and $Na_3PO_3S{\cdot}12H_2O$ with partial occupations of P, S, or O atoms.[28] The excluded hydrates include more H_2O molecules, and they should possess higher Gibbs energies of reaction according to the results shown in section 3.2. Finally, nine kinds of reaction products (P#1/As#1 to P#9/As#9) and the corresponding nine reactions (R1−R9) were considered in the present work; see Table 2. These reaction products can be grouped into three categories: (i) oxysulfides Na_3MOS_3, $Na_3MO_2S_2$, and Na_3MO_3S (M = As or P, and similarly hereinafter) with H_2S release from reactions R1−R3, (ii) hydrates

Table 2. Possible Reactions of Na_3MS_4 (M = P or As) with H_2O by Examining the ICSD (Inorganic Crystal Structure Database)[26]

group	no.	name[a]	reaction (M = P or As)
1	R1	P#1 or As#1	$Na_3MS_4 + H_2O \rightleftarrows Na_3MOS_3 + H_2S$
	R2	P#2 or As#2	$Na_3MS_4 + 2\ H_2O \rightleftarrows Na_3MO_2S_2 + 2\ H_2S$
	R3	P#3 or As#3	$Na_3MS_4 + 3\ H_2O \rightleftarrows Na_3MO_3S + 3\ H_2S$
2	R4	P#4 or As#4	$Na_3MS_4 + 8\ H_2O \rightleftarrows Na_3MS_4{\cdot}8H_2O$
	R5	P#5 or As#5	$Na_3MS_4 + 9\ H_2O \rightleftarrows Na_3MS_4{\cdot}9H_2O$
3	R6	P#6 or As#6	$Na_3MS_4 + 10\ H_2O \rightleftarrows Na_3MO_3S{\cdot}7H_2O + 3H_2S$
	R7	P#7 or As#7	$Na_3MS_4 + 12\ H_2O \rightleftarrows Na_3MOS_3{\cdot}11H_2O + H_2S$
	R8	P#8 or As#8	$Na_3MS_4 + 13\ H_2O \rightleftarrows Na_3MO_2S_2{\cdot}11H_2O + 2H_2S$
	R9	P#9 or As#9	$Na_3MS_4 + 15\ H_2O \rightleftarrows Na_3MO_3S{\cdot}12H_2O + 3H_2S$

[a]Name for the reaction product which is not H_2S, such as P#1 for Na_3POS_3; see details in Table S1 (Supporting Information).

DOI: 10.1021/acsami.7b03606
ACS Appl. Mater. Interfaces 2017, 9, 16261−16269

$Na_3MS_4·8H_2O$ and $Na_3MS_4·9H_2O$ from reactions R4 and R5, and (iii) oxysulfide hydrates from a combination of the above two, i.e., $Na_3MO_3S·7H_2O$, $Na_3MOS_3·11H_2O$, $Na_3MO_2S_2·11H_2O$, and $Na_3MO_3S·12H_2O$ from reactions R6−R9. Structural details of these compounds (see Table 2) are given in Table S1.

Regarding H_2O and H_2S in reactions 1 and 2 as well as Table 2, the thermodynamically stable phases under low temperature and pressure conditions were selected, i.e., ice XI[29] and orthorhombic H_2S (solid)[30] as detailed in Table S1.

It is worth mentioning that the present analyses of moisture stability were carried out at 0 K, and it was found that the predicted reaction Gibbs energies at 0 K are good enough to explore the enhanced moisture stability in $Na_3P_{1-x}As_xS_4$ at room temperature due to the effect of the alloying element arsenic. In fact, first-principles energies predicted at 0 K can be used satisfactorily to represent the (relative) Gibbs energies at low temperatures (such as room temperature) because of the limited effect or the cancellation of entropy at these temperatures. When Gibbs energies at finite temperatures are needed for materials which are difficult to calculate, such as liquid H_2O, an effective way is to use the measured thermodynamic data in combination with the easily calculated DFT data; see the recent works for battery materials.[31,32] In addition, when aqueous stability as a function of the pH value is the major concern, the Pourbaix diagram can be employed.[32,33]

2.3. First-Principles and Phonon Calculations. *2.3.1. First-Principles Calculations.* All DFT-based first-principles calculations were performed by the Vienna Ab initio Simulation Package (VASP 5.4.1)[34,35] with the ion−electron interaction depicted using the projector augmented wave method.[36] Four exchange-correction (X-C) functionals were employed and examined starting from our previous DFT work for sulfur-containing materials.[37] These X-C functionals include (i) the generalized gradient approximation (GGA) developed by Perdew, Burke, and Ernzerhof (PBE),[38] (ii) the improved GGA-PBE for densely packed solids and their surfaces (PBEsol, or PS for simplicity),[39] and (iii and iv) the semiempirical van der Waals correction as implemented by Grimme et al. (the D3 method),[40] i.e., the PBE+D3 and PS+D3 methods. More details of first-principles calculations are given in the Supporting Information, including structural details for each compound, the *k*-point mesh, the cutoff energy, and smearing methods for structural relaxation and an accurate total energy.

2.3.2. Phonon Calculations. Concerning the present polar material of $Na_3P_{1-x}As_xS_4$, we used a parameter-free mixed-space approach[41] as implemented in the YPHON code[42] for phonon calculations, which accounts for the long-range dipole−dipole interactions resulting in the well-known longitudinal optical and transverse optical (LO−TO) splitting; see details in our review paper.[43] Here, the VASP code was again the computational engine to obtain the force constants, i.e., the Hessian matrix, in terms of the density functional perturbation theory. Other details including the supercell size, *k*-point mesh, and cutoff energy are given in the Supporting Information.

2.3.3. Thermodynamics. The quasiharmonic approach in terms of first-principles and phonon calculations was used to calculate the Helmholtz energy F for a given structure under volume V and temperature T:[44,45]

$$F(V, T) = E_c(V) + F_{vib}(V, T) + F_{el}(V, T) \quad (3)$$

F_{vib} is the vibrational contribution by phonon calculations using data at four to six volumes. F_{el} is the thermal electronic contribution for metals; it was ignored herein due to the semiconductor and insulator nature of $Na_3P_{1-x}As_xS_4$. E_c is the static total energy at 0 K without the zero-point vibrational energy (ZPE) calculated by VASP. $E_c(V)$ was determined by fitting the first-principles energy versus volume (E−V) data points according to a four-parameter Birch−Murnaghan equation of state (EOS):[45]

$$E(V) = a_1 + a_2V^{-2/3} + a_3V^{-4/3} + a_4V^{-2} \quad (4)$$

where a_1, a_2, a_3, and a_4 are fitting parameters. Correspondingly, the pressure−volume (P−V) EOS can be obtained by $P = -dE/dV$.[37] Equilibrium properties determined from EOS fittings include the energy (E_0), volume (V_0), bulk modulus (B_0), and first derivative of the bulk modulus with respect to pressure (B'). Six to eight data points within the volume range of $-10\% < (V - V_0)/V_0 < +10\%$ were typically used for the present EOS fittings.

3. RESULTS AND DISCUSSION

3.1. Structural and Phonon Properties of $Na_3P_{1-x}As_xS_4$. Before discussing phase stability, we show first the capability of first-principles calculations in predicting the structural and phonon properties of $Na_3P_{1-x}As_xS_4$.

3.1.1. Structural Properties. Figure 1 shows a comparison of experimental equilibrium volumes with respect to first-principles predictions by using different X-C functionals for $Na_3P_{1-x}As_xS_4$ and associated compounds as listed in Table 2. All the data shown in Figure 1 are also given in Table S2 (Supporting Information). In general, the predicted equilibrium volumes (V) show the trend of $V_{PBE} > V_{PBE+D3} \approx V_{PS} > V_{PS+D3}$, and the predicted V_{PBE+D3} and V_{PS} are closer to experimental data except for H_2O (ice XI), with the better prediction being for V_{PBE}. In addition, the present V_{PBE} values from E−V EOS fitting, see eq 4, agree reasonably well with the directly relaxed V_{PBE} values in the Materials Project database.[23,24] The largest exception is for H_2S due to the significant difference in predicting the equilibrium volume from energy (such as the present E−V EOS fitting) and stress (such as the direct relaxation by the Materials Project and the present P−V EOS fitting) for some materials.[46,47] It is believed that the results from energy are more accurate since stress is an indirect first-principles output via the derivative of energy. The first-principles results shown in Figure 1 indicate that both PS and PBE+D3 are more suitable to describe $Na_3P_{1-x}As_xS_4$ and associated compounds from the viewpoint of equilibrium volume.

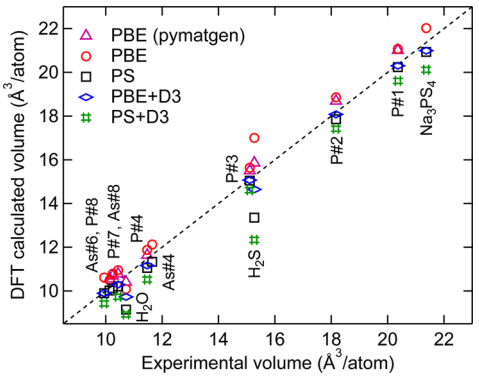

Figure 1. First-principles-predicted equilibrium volumes by different X-C functionals in comparison with experimental data. DFT data in the literature (i.e., the Materials Project)[23,24] are also listed. Structural details and all the used data are given in Tables S1 and S2, respectively (Supporting Information).

Besides the equilibrium volume, very little experimental information on the bulk modulus (B_0) and its pressure derivative (B') is available for $Na_3P_{1-x}As_xS_4$ and associated compounds, except for ice XI and solid H_2S; see Table S2. The predicted B_0 values (15.2−23.0 GPa) for ice XI are larger than the measurement (8.9 GPa) at 257 K[48] due mainly to the smaller volumes from first-principles calculations; see Table S2. Regarding solid H_2S, the predicted B_0 value (3.1 GPa from PBE) agrees reasonably well with the roughly estimated value

DOI: 10.1021/acsami.7b03606
ACS Appl. Mater. Interfaces 2017, 9, 16261−16269

(<3 GPa) using the measured elastic constants at pressure >0.5 GPa;[49,50] see Table S2. Regarding the tetragonal $Na_3P_{1-x}As_xS_4$, Figure S1a (Supporting Information) shows that the predicted B' values are around 4.9—a normal value for most materials.[46] Figure S1b shows that the equilibrium volume of $Na_3P_{1-x}As_xS_4$ increases almost linearly from 20.936 to 21.568 Å^3/atom with increasing As concentration, and correspondingly, the bulk modulus B_0 decreases from 25.7 to 24.4 GPa due to the addition of As (see also Table S2), indicating that the alloying element As makes Na_3PS_4 softer.

3.1.2. Phonon Properties. Figure 2 shows the predicted phonon dispersions and densities of states (DOSs) for

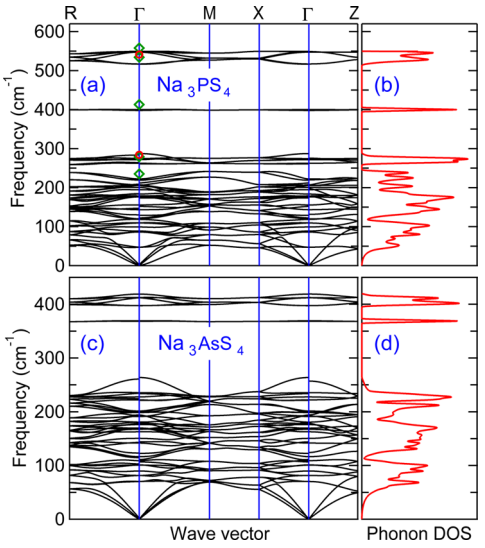

Figure 2. First-principles-predicted phonon dispersion curves and phonon densities of states (DOSs) with the LO−TO splitting included for tetragonal Na_3PS_4 (panels a and b, respectively) and Na_3AsS_4 (panels c and d, respectively) in terms of the X-C functional of PS (PBEsol). Measured Raman (tilted squares) and infrared (circles) data at the Γ point are also shown for Na_3PS_4;[51] see detailed comparisons in Table S3 (Supporting Information).

tetragonal Na_3PS_4 and Na_3AsS_4 using the X-C functional of PS (PBEsol). Correspondingly, the predicted partial phonon DOSs are shown in Figure S2 (Supporting Information). It is worth mentioning that the inequality of vibrational frequencies along different directions to the Γ point is due to the effect of LO−TO splitting. Figure 2a shows that the predicted phonon frequencies at the Γ point of Na_3PS_4 agree reasonably well with the Raman and infrared measurements.[51] Details about the predicted phonon frequencies at Γ point are given in Table S3 (Supporting Information) for tetragonal Na_3PS_4 and Na_3AsS_4 in comparison with experimental data when available. No imaginary phonon modes appear in Figure 2, indicating that both Na_3PS_4 and Na_3AsS_4 are stable or metastable, agreeing with experimental observations.[52,53] In general, the shapes of phonon dispersions and DOSs for Na_3PS_4 and Na_3AsS_4 are similar (see Figure 2). However, phonon frequencies of Na_3AsS_4 (such as around 410 and 360 cm^{-1}) are much lower than the corresponding frequencies of Na_3PS_4 (around 540 and 450 cm^{-1}) due to the weaker As−S bonding compared to the P−S bonding; see Figure S2 for the As−S and P−S phonon hybridizations. The weaker As−S bonding is consistent with the lower As−S force constants[12] and the softer nature of Na_3AsS_4 with respect to Na_3PS_4 (see the bulk moduli of Na_3PS_4 and Na_3AsS_4 in Table S2).

Besides the phonon DOSs for the two end members Na_3PS_4 and Na_3AsS_4, first-principles-predicted phonon DOSs for the low- and high-energy structures of $Na_3P_{0.5}As_{0.5}S_4$ are also plotted in Figure S3 in comparison with those of Na_3PS_4 and Na_3AsS_4, indicating the similar shapes of phonon DOSs, especially between $Na_3P_{0.5}As_{0.5}S_4$ and Na_3AsS_4.

3.2. Phase Stability of $Na_3P_{1-x}As_xS_4$ at 0 K and Finite Temperatures. Figure 3 shows the first-principles-predicted

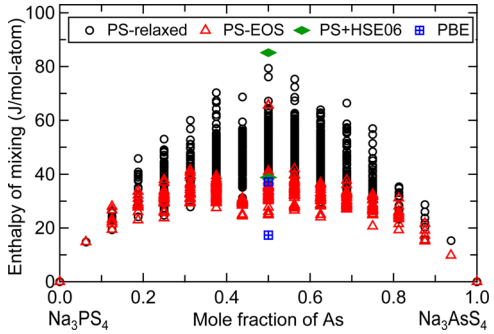

Figure 3. First-principles-predicted enthalpy of mixing by using different X-C functionals (PS, PBE, and PS+HSE06) and methods (EOS fitting and direct DFT relaxations).

enthalpy of mixing for $Na_3P_{1-x}As_xS_4$ in terms of the 128-atom supercell and without the ZPE effect. Here, the X-C functional of PS is employed together with auxiliary examinations by PBE and PS+HSE06 (a hybrid functional[54] as shown previously[12]) for the low- and high-energy structures of $Na_3P_{0.5}As_{0.5}S_4$. It is seen that $Na_3P_{1-x}As_xS_4$ has a positive enthalpy of mixing predicted by different X-C functionals, indicating the existence of a miscibility gap and hence phase separation. However, Figure 3 also shows that the values of enthalpy of mixing are quite small (<0.1 kJ/mol-atom or 1 meV/atom even when x = 0.5), indicating that $Na_3P_{1-x}As_xS_4$ can be stable at higher temperatures. The estimated consolute temperature of the $Na_3P_{1-x}As_xS_4$ miscibility gap is around 100 K in terms of the mean field theory and the ideal mixing approach, indicating $Na_3P_{1-x}As_xS_4$ is stable above ∼100 K on the basis of the configurational entropy only, where the detailed predictions were shown in our previous work.[12]

Figure 4 shows the vibrational Gibbs energy differences for the low- and high-energy structures of $Na_3P_{0.5}As_{0.5}S_4$ in terms of the quasiharmonic phonon approach, see eq 3, and the X-C functional of PS (PBEsol). Note that (i) the reference states are tetragonal Na_3PS_4 and Na_3AsS_4 and (ii) the static energy differences at 0 K are excluded (see Figure 3). The vibrational entropies and Gibbs energies are given in Table S4 (Supporting Information) at selected temperatures for $Na_3P_{1-x}As_xS_4$ (x = 0, 0.5, and 1). The Gibbs energies at 0 K are ZPEs (3.859, 3.581, 3.523, and 3.361 kJ/mol-atom), which decrease with increasing As concentration since the mass of the element As is heavier than that of the element P, and Na_3AsS_4 is softer than that of Na_3PS_4 as discussed previously. Figure 4 shows that the vibrational Gibbs energy difference of $Na_3P_{0.5}As_{0.5}S_4$ decreases with increasing temperature. At 0 K, the vibrational Gibbs energy difference for $Na_3P_{0.5}As_{0.5}S_4$ is about −0.5 kJ/mol-atom due to ZPEs, which is comparable to the static enthalpy of mixing (see Figure 3), implying that $Na_3P_{1-x}As_xS_4$ is stable at 0 K due to the zero-point vibrational energy.

DOI: 10.1021/acsami.7b03606
ACS Appl. Mater. Interfaces 2017, 9, 16261−16269

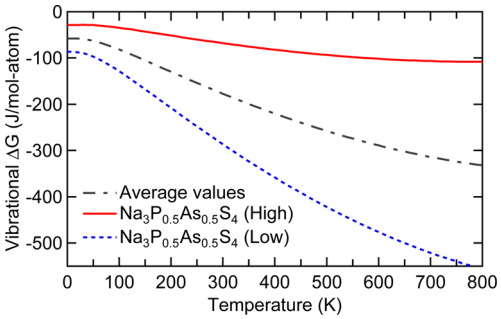

Figure 4. Vibrational Gibbs energy differences for a low-energy phase and a high-energy phase of $Na_3P_{0.5}As_{0.5}S_4$ (structures reported previously[12]) in terms of the quasiharmonic phonon approach using the X-C functional of PS (PBEsol). Note that the reference states are Na_3PS_4 and Na_3AsS_4 and the static energy differences at 0 K are excluded.

The above discussion indicates that $Na_3P_{1-x}As_xS_4$ is a superionic conductor stabilized at 0 K by zero-point vibrational energy, albeit it has a slightly positive enthalpy of mixing at 0 K, and $Na_3P_{1-x}As_xS_4$ becomes more and more stable at finite temperatures due to both the vibrational entropy and the configurational entropy. It is expected that the effect on the Gibbs energy from configurational entropy becomes more significant than that from vibrational entropy with increasing temperature, especially when the As concentration $x \approx 0.5$.

3.3. Air and Moisture Stability of $Na_3P_{1-x}As_xS_4$. Similar to the cases of $Li_{3.833}Sn_{0.833}As_{0.166}S_4$[6] and Na_3SbS_4,[7] $Na_3P_{1-x}As_xS_4$ is dry-air stable. For example, no obvious changes are observed in the XRD patterns of Na_3PS_4 before and after exposure to air at 413 K (140 °C) for 100 h (see Figure S4, Supporting Information), indicating that Na_3PS_4 is stable with respect to oxygen. However, Na_3PS_4 is moisture unstable when it is exposed in air for 1.5 h with 25% humidity at room temperature on the basis of XRD measurements (not shown), and the H_2S gas was detected immediately after air exposure at room temperature with 45% humidity.[12] As an example, Figure 5 shows the XRD patterns of powder Na_3PS_4 before and after air exposure at room temperature with 15% humidity for 100 h. After exposure, four extra XRD peaks (nos. 1, 2, 5, and 6 marked in Figure 5) and two enhanced peaks (nos. 3 and 4) appear, indicating the formation of new phases. The powder

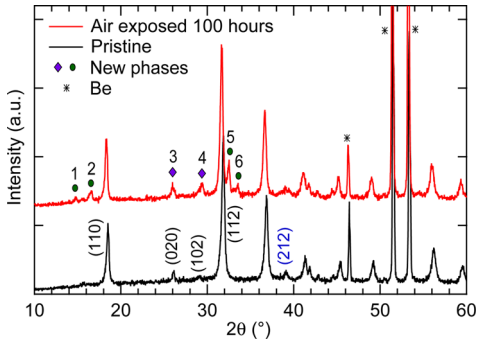

Figure 5. Measured XRD (Cu Kα) patterns of powder Na_3PS_4 before and after air exposure at room temperature with 15% humidity for 100 h, where beryllium (Be) is used as the air-sensitive holder. Note that we reported the similar XRD patterns previously,[12] where only four, instead of six, peaks relevant to the new phases were marked due to lack of confidence previously.

SEM images in Figure 6 indicate that the particle sizes are similar before and after air exposure with 15% humidity for 100 h; however, the particle shape is sharper in the pristine Na_3PS_4, and after air exposure it looks like the particle surface is covered by a layer of coating, making the particle shape blunt. As a result, the Na ion conductivity decreases from 0.2 mS/cm for the pristine Na_3PS_4 to 0.05−0.1 mS/cm for the exposed Na_3PS_4 according to the impedance measurements.[12] With increasing As concentration, the moisture stability of $Na_3P_{1-x}As_xS_4$ is enhanced; for instance, no new XRD peaks were observed in $Na_3P_{0.62}As_{0.38}S_4$ exposed to moisture with 15% humidity for 100 h.[12]

To understand the enhanced moisture stability in $Na_3P_{1-x}As_xS_4$, Figure 7 shows the first-principles-predicted Gibbs energies of reaction (ΔG_r) at 0 K for $Na_3MS_4 + H_2O$ (M = P or As); see Table 2 for these reactions and Table S2 for the present first-principles results. Note that the Materials Project values[23,24] (relaxed results using PBE) are also listed in Table S2 when available, which agree reasonably well with the present PBE results from the EOS fittings except for As#6 ($Na_3AsO_3S\cdot 7H_2O$), P#7 ($Na_3POS_3\cdot 11H_2O$), and P#9 ($Na_3PO_3S\cdot 12H_2O$) with an energy difference of >2 meV/atom. The energy deviations between the present PBE calculations and the Materials Project values have contributions from the different *k*-point meshes employed (such as 2 × 2 × 2 for P#7 by the Materials Project; while more *k*-point meshes were used in the present cases; see Table S1).

Figure 7 shows that the lowest ΔG_r value at 0 K for "$Na_3PS_4 + H_2O$" is from reaction R1 with the reaction products of "$Na_3POS_3 + H_2S$", followed by reaction R2 with the reaction products "$Na_3PO_2S_2 + H_2S$". The ΔG_r values are relatively higher for formation of the hydrates, especially the oxysulfide hydrates with more H_2O molecules (see also Table S2). Experimentally, these hydrates can be synthesized in aqueous solution,[55,56] and the absorbed H_2O will be lost from these hydrates on heating or freeze-drying.[57] Concerning "$Na_3AsS_4 + H_2O$", the lowest ΔG_r value—different from the above Na_3PS_4 case—is from reaction R4 (or R5) with the reaction product of $Na_3AsS_4\cdot 8H_2O$ (or $Na_3AsS_4\cdot 9H_2O$). From reaction R1 of "$Na_3PS_4 + H_2O$" to reaction R4/R5 of "$Na_3AsS_4 + H_2O$", Figure 7 and Table S2 show that the ΔG_r value increases by 1.9 kJ/mol-atom (PBE) or 1.5 kJ/mol-atom (PS), indicating the enhanced moisture stability with increasing As content. To further investigate "$Na_3P_{1-x}As_xS_4 + H_2O$" as a function of the alloying element arsenic, the enthalpies of mixing for $Na_3P_{1-x}As_xS_4$ and associated reaction products need to be considered. Similar to the $Na_3P_{1-x}As_xS_4$ case in Figure 3, it is found that the values of the enthalpy of mixing are also negligibly small for the examined compounds $Na_3P_{1-x}As_xOS_3$ (<0.08 kJ/mol-atom or 0.8 meV/atom) and $Na_3P_{1-x}As_xS_4\cdot 8H_2O$ (<0.01 kJ/mol-atom or 0.1 meV/atom); see the data reported in Table S5 (Supporting Information). It is hence reasonable to estimate the ΔG_r values of "$Na_3P_{1-x}As_xS_4 + H_2O$" using the ideal mixing approach by ignoring the enthalpy of mixing.

Figure 8 shows the PBE- and PS-predicted ΔG_r values at 0 K and without ZPE for "$Na_3P_{1-x}As_xS_4 + H_2O$" according to the aforementioned ideal mixing approach. Both PBE and PS give similar results, and the PBE results will be discussed mainly. Similar to the observations in Figure 7, Figure 8 shows that the possible reaction products are oxysulfides $Na_3P_{1-x}As_xOS_3$, $Na_3P_{1-x}As_xO_2S_2$, and $Na_3P_{1-x}As_xO_3S$ when $x < \sim 0.25$. At higher arsenic contents, such as those indicated by the green

DOI: 10.1021/acsami.7b03606
ACS Appl. Mater. Interfaces 2017, 9, 16261−16269

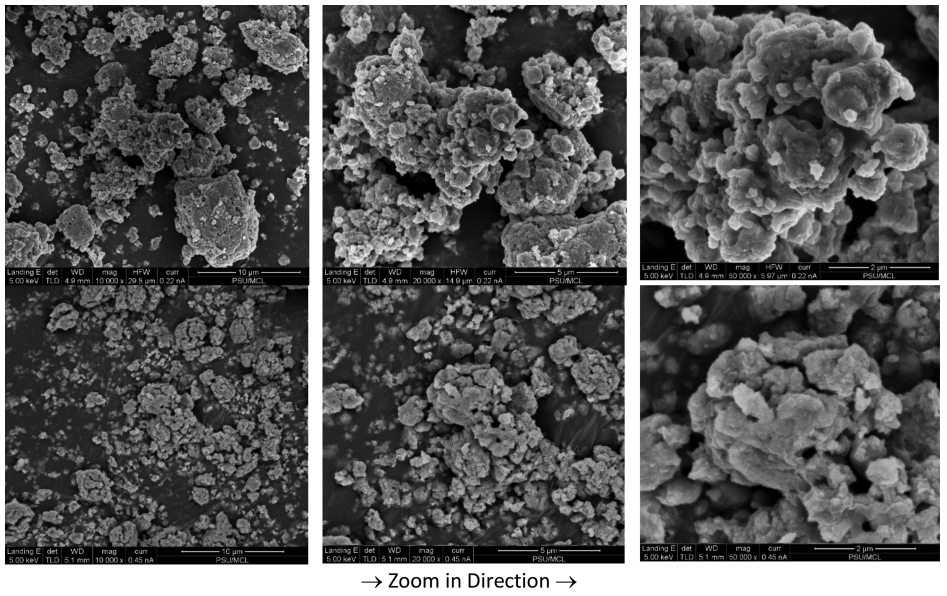

Figure 6. Powder SEM images of Na_3PS_4 before (three images above) and after (three images below) air exposure at room temperature with 15% humidity for 100 h. Note that the zoom-in direction is from left to right.

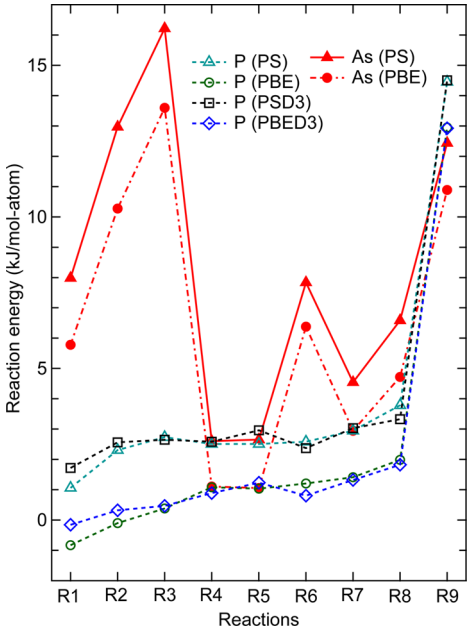

Figure 7. First-principles-predicted reaction Gibbs energies of Na_3MS_4 + H_2O (M = P or As) at 0 K (without ZPE) for the reactions (R1−R9) listed in Table 2. All data used in this figure are also given in Table S2 (Supporting Information).

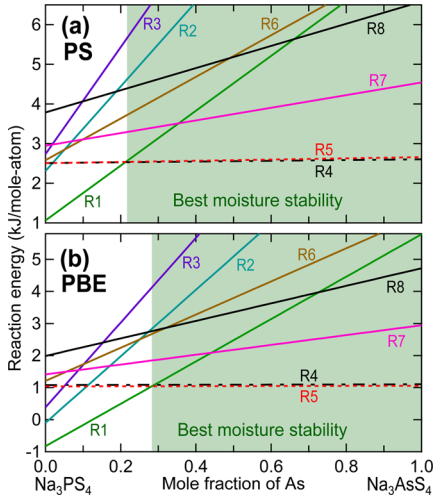

Figure 8. First-principles-predicted reaction Gibbs energies ΔG_r at 0 K (without ZPE) as a function of the As concentration using the X-C functionals of (a) PS and (b) PBE. Reactions R1−R9 are shown in Table 2, and the highlighted regions indicate that $Na_3P_{1-x}As_xS_4$ (x > ~0.25) has the best moisture (H_2O) stability with the highest ΔG_r values.

highlighted region, with x > ~0.25 (i.e., >0.28 by PBE and >0.22 by PS), $Na_3P_{1-x}As_xS_4$ reaches the best moisture stability region, i.e., the region with the highest ΔG_r values. In this region, the hydrates ($Na_3P_xAs_{1-x}S_4 \cdot nH_2O$ with n = 8 and/or 9) are the possible reaction products with high ΔG_r values (e.g., >~1 kJ/mol-atom for the PBE case).

It was shown that the high As-containing $Na_3P_{1-x}As_xS_4$ (e.g., $Na_3P_{0.62}As_{0.38}S_4$) is moisture stable after exposure to air with 15% humidity at room temperature for 100 h.[12] To identify the moisture products for the low-As-containing $Na_3P_{1-x}As_xS_4$, we examine the XRD patterns of the air-exposed Na_3PS_4 with 15% humidity for 100 h (Figure 5) and the simulated XRD patterns for Na_3PS_4, Na_3POS_3, $Na_3PO_2S_2$, and Na_3PO_3S in terms of the structures reported in the literature;[20,58,57,59] see Figure S5. It is concluded that the most possible reaction products at room temperature from "Na_3PS_4 + H_2O" are Na_3POS_3 (P#1) and $Na_3PO_2S_2$ (P#2) according to the following observations. The new peak 1 in Figure 5 originates from the (210) diffraction of P#2, confirmed by the enhanced peak 3 due to the (420) superlattice diffraction of P#2. The new peak 2 in Figure 5 stems from the (020) diffractions of P#1 and P#2, confirmed by the enhanced peak 4 due to the (040) superlattice diffraction of P#1 and the new peak 5 due to the (040) superlattice diffraction of P#2. The new peak 6 in Figure 5 may arise from the (311) diffraction of P#1 and/or the (014) diffraction of P#3; however, we cannot confirm its origin due to the limited information in Figure 5.

DOI: 10.1021/acsami.7b03606
ACS Appl. Mater. Interfaces 2017, 9, 16261−16269

The above experimental and first-principles results show that a rough ΔG_r value (>∼ 1.0 kJ/mol-atom from PBE calculations) can be used to judge the stability of "$Na_3P_{1-x}As_xS_4$ + H_2O" under nonheavy moisture (such as 15% humidity). This ΔG_r value agrees reasonably well with the observed reactions, which slowly take place at a temperature near 0 °C:[60]

$$Na_3PS_4 + 3H_2O \rightarrow Na_3PO_3S\ (P\#3) + 3H_2S \quad (5)$$

$$Na_3PO_2S_2\ (P\#1) + Na_3POS_3\ (P\#2) + 3H_2O \rightarrow 2Na_3PO_3S\ (P\#3) + 3H_2S \quad (6)$$

On the basis of the present first-principles data by PBE shown in Table S2, ΔG_r = 0.38 kJ/mol-atom for reaction 5 and ΔG_r = 0.94 kJ/mol-atom for reaction 6, which are less than 1.0 kJ/mol-atom.

The present work indicates that the enhanced moisture stability of $Na_3P_{1-x}As_xS_4$ stems from the shift of the reaction products from the easy-forming oxysulfides with lower ΔG_r values (such as $Na_3P_{1-x}As_xOS_3$ and $Na_3P_{1-x}As_xO_2S_2$ with H_2S release when $x < 0.25$) to the relatively difficult-forming hydrates with higher ΔG_r values (such as $Na_3P_{1-x}As_xS_4{\cdot}8H_2O$ and $Na_3P_{1-x}As_xS_4{\cdot}9H_2O$ with $x > 0.25$). These shifts can be understood by the weaker As−O affinity with respect to P−O, making it difficult to form oxysulfides with increasing As concentration. For example, the bond dissociation energies in diatomic As−O and P−O molecules are 484 and 589 kJ/mol, respectively; and the bond dissociation energies in diatomic As−O and P−O cations are 495 and 791 kJ/mol, respectively.[61] The weaker As−O affinity is also reflected in the lower bulk moduli in As-containing oxysulfides, such as 26.1 GPa (for compound P#1, PBE result as shown in Table S2) vs 23.8 GPa (As#1), 26.7 GPa (P#2) vs 23.5 GPa (As#2), and 37.4 GPa (P#3) vs 34.6 GPa (As#3). However, the bulk moduli of As-containing hydrates are comparable to and even higher than those of the P-containing hydrates, for example, 16.9 GPa (PBE result of P#4) vs 17.5 GPa (As#4); see more results in Table S2.

It should be remarked that $Na_3P_{1-x}As_xS_4$ ($0 \le x \le 1$) is unstable under heavy moisture. For example, our examination[12] indicated that the H_2S gas was released immediately when Na_3PS_4 was exposed to air at room temperature with 45% humidity, and the H_2S gas was also released after 6 min for the case of $Na_3P_{0.62}As_{0.38}S_4$ under the same condition.

4. CONCLUSIONS

In the present work we investigated the origin of the outstanding phase stability and the enhanced moisture stability in a $Na_3P_{1-x}As_xS_4$ superionic conductor by means of first-principles and phonon calculations with verifications from experiments. In addition to an exceptionally high Na ion conductivity achieved in $Na_3P_{0.62}As_{0.38}S_4$ by tailoring the alloying element arsenic,[12] the present work shows that more innovations can be fulfilled for Na_3PS_4-type solid-state electrolytes via the alloying element arsenic. The present work reveals that (i) $Na_3P_{1-x}As_xS_4$ ($0 \le x \le 1$) is a solid-state superionic conductor stabilized at 0 K by zero-point vibrational energy, albeit it has a positive enthalpy of mixing, and $Na_3P_{1-x}As_xS_4$ becomes more stable at finite temperatures because of the vibrational and configurational entropies and (ii) $Na_3P_{1-x}As_xS_4$ possesses pronounced moisture (i.e., H_2O) stability when $x >$ ∼0.25 due to the shift of reaction products from the easy-forming oxysulfides (for example, $Na_3P_{1-x}As_xOS_3$ and $Na_3P_{1-x}As_xO_2S_2$ with H_2S release) to the difficult-forming hydrates (for example, $Na_3P_{1-x}As_xS_4{\cdot}nH_2O$ with n = 8 and/or 9) because of the weaker As−O affinity with respect to that of P−O. The present work shows that alloying is able to achieve multiple innovations in superionic conductors, for example, a combination of high ionic conductivity with excellent stability with respect to temperature, composition, and atmosphere (e.g., H_2O and O_2).

■ ASSOCIATED CONTENT

Supporting Information

The Supporting Information is available free of charge on the ACS Publications website at DOI: 10.1021/acsami.7b03606.

Additional computational details, structural information, first-principles results from EOS fittings for all alloys and compounds considered in the present work, phonon frequencies at the Γ point and partial phonon DOSs for tetragonal Na_3PS_4 and Na_3AsS_4, vibrational Gibbs energy and entropy for $Na_3P_xAs_{1-x}S_4$, XRD patterns of Na_3PS_4 before and after air exposure at 140 °C for 100 h, and calculated XRD patterns for Na_3PS_4, Na_3POS_3, $Na_3PO_2S_2$, and Na_3PO_3S (PDF)

■ AUTHOR INFORMATION

Corresponding Author

*E-mail: sus26@psu.edu.

ORCID

Shun-Li Shang: 0000-0002-6524-8897
Yi Wang: 0000-0001-6154-945X
Donghai Wang: 0000-0001-7261-8510

Notes

The authors declare no competing financial interest.

■ ACKNOWLEDGMENTS

We acknowledge financial support from the National Science Foundation (NSF) with Grant Nos. DMR-1310289 and DMR-1610430 and the ICS (Institute for CyberScience) Seed Grant from The Pennsylvania State University. First-principles calculations were carried out partially on the LION clusters at The Pennsylvania State University, partially on the resources of the NERSC (National Energy Research Scientific Computing Center) supported by the Office of Science of the U.S. Department of Energy under Contract No. DE-AC02-05CH11231, and partially on the resources of XSEDE (Extreme Science and Engineering Discovery Environment) supported by the NSF with Grant No. ACI-1053575.

■ REFERENCES

(1) Kundu, D.; Talaie, E.; Duffort, V.; Nazar, L. F. The Emerging Chemistry of Sodium Ion Batteries for Electrochemical Energy Storage. *Angew. Chem., Int. Ed.* **2015**, *54*, 3431−3448.
(2) Manthiram, A.; Yu, X. Ambient Temperature Sodium-Sulfur Batteries. *Small* **2015**, *11*, 2108−2114.
(3) Yabuuchi, N.; Kubota, K.; Dahbi, M.; Komaba, S. Research Development on Sodium-Ion Batteries. *Chem. Rev.* **2014**, *114*, 11636−11682.
(4) Ponrouch, A.; Monti, D.; Boschin, A.; Steen, B.; Johansson, P.; Palacín, M. R. Non-Aqueous Electrolytes for Sodium-Ion Batteries. *J. Mater. Chem. A* **2015**, *3*, 22−42.
(5) Oshima, T.; Kajita, M.; Okuno, A. Development of Sodium-Sulfur Batteries. *Int. J. Appl. Ceram. Technol.* **2004**, *1*, 269−276.

DOI: 10.1021/acsami.7b03606
ACS Appl. Mater. Interfaces 2017, 9, 16261−16269

(6) Sahu, G.; Lin, Z.; Li, J.; Liu, Z.; Dudney, N.; Liang, C. Air-Stable, High-Conduction Solid Electrolytes of Arsenic-Substituted Li_4SnS_4. *Energy Environ. Sci.* **2014**, *7*, 1053−1058.
(7) Banerjee, A.; Park, K. H.; Heo, J. W.; Nam, Y. J.; Moon, C. K.; Oh, S. M.; Hong, S.-T.; Jung, Y. S. Na_3SbS_4: A Solution Processable Sodium Superionic Conductor for All-Solid-State Sodium-Ion Batteries. *Angew. Chem.* **2016**, *128*, 9786−9790.
(8) Kamaya, N.; Homma, K.; Yamakawa, Y.; Hirayama, M.; Kanno, R.; Yonemura, M.; Kamiyama, T.; Kato, Y.; Hama, S.; Kawamoto, K.; Mitsui, A. A Lithium Superionic Conductor. *Nat. Mater.* **2011**, *10*, 682−686.
(9) Kato, Y.; Hori, S.; Saito, T.; Suzuki, K.; Hirayama, M.; Mitsui, A.; Yonemura, M.; Iba, H.; Kanno, R. High-Power All-Solid-State Batteries Using Sulfide Superionic Conductors. *Nat. Energy* **2016**, *1*, 16030.
(10) Hayashi, A.; Noi, K.; Sakuda, A.; Tatsumisago, M. Superionic Glass-Ceramic Electrolytes for Room-Temperature Rechargeable Sodium Batteries. *Nat. Commun.* **2012**, *3*, 856.
(11) Hayashi, A.; Noi, K.; Tanibata, N.; Nagao, M.; Tatsumisago, M. High Sodium Ion Conductivity of Glass−Ceramic Electrolytes with Cubic Na_3PS_4. *J. Power Sources* **2014**, *258*, 420−423.
(12) Yu, Z.; Shang, S.-L.; Seo, J.-H.; Wang, D.; Luo, X.; Huang, Q.; Chen, S.; Lu, J.; Li, X.; Liu, Z.-K.; Wang, D. Exceptionally High Ionic Conductivity in $Na_3P_{0.62}As_{0.38}S_4$ with Improved Moisture Stability for Solid-State Sodium-Ion Batteries. *Adv. Mater.* **2017**, *29*, 1605561.
(13) Zhang, L.; Yang, K.; Mi, J. L.; Lu, L.; Zhao, L. R.; Wang, L. M.; Li, Y. M.; Zeng, H. Na_3PSe_4: A Novel Chalcogenide Solid Electrolyte with High Ionic Conductivity. *Adv. Energy Mater.* **2015**, *5*, 1501294.
(14) Chu, I.-H.; Kompella, C. S.; Nguyen, H.; Zhu, Z.; Hy, S.; Deng, Z.; Meng, Y. S.; Ong, S. P. Room-Temperature All-Solid-State Rechargeable Sodium-Ion Batteries with a Cl-Doped Na_3PS_4 Superionic Conductor. *Sci. Rep.* **2016**, *6*, 33733.
(15) Tanibata, N.; Noi, K.; Hayashi, A.; Tatsumisago, M. Preparation and Characterization of Highly Sodium Ion Conducting Na_3PS_4-Na_4SiS_4 Solid Electrolytes. *RSC Adv.* **2014**, *4*, 17120.
(16) Richards, W. D.; Tsujimura, T.; Miara, L. J.; Wang, Y.; Kim, J. C.; Ong, S. P.; Uechi, I.; Suzuki, N.; Ceder, G. Design and Synthesis of the Superionic Conductor $Na_{10}SnP_2S_{12}$. *Nat. Commun.* **2016**, *7*, 11009.
(17) Zhu, Z. Y.; Chu, I.-H.; Deng, Z.; Ong, S. P. Role of Na^+ Interstitials and Dopants in Enhancing the Na^+ Conductivity of the Cubic Na_3PS_4 Superionic Conductor. *Chem. Mater.* **2015**, *27*, 8318−8325.
(18) Ponrouch, A.; Marchante, E.; Courty, M.; Tarascon, J.-M.; Palacín, M. R. In Search of an Optimized Electrolyte for Na-Ion Batteries. *Energy Environ. Sci.* **2012**, *5*, 8572.
(19) Grey, C. P.; Tarascon, J. M. Sustainability and in Situ Monitoring in Battery Development. *Nat. Mater.* **2016**, *16*, 45−56.
(20) Jansen, M.; Henseler, U. Synthesis, Structure Determination, and Ionic-Conductivity of Sodium Tetrathiophosphate. *J. Solid State Chem.* **1992**, *99*, 110−119.
(21) Tanibata, N.; Noi, K.; Hayashi, A.; Kitamura, N.; Idemoto, Y.; Tatsumisago, M. X-Ray Crystal Structure Analysis of Sodium-Ion Conductivity in $94Na_3PS_4$-$6Na_4SiS_4$ Glass-Ceramic Electrolytes. *ChemElectroChem* **2014**, *1*, 1130−1132.
(22) van de Walle, A. Multicomponent Multisublattice Alloys, Nonconfigurational Entropy and Other Additions to the Alloy Theoretic Automated Toolkit. *CALPHAD: Comput. Coupling Phase Diagrams Thermochem.* **2009**, *33*, 266−278.
(23) Jain, A.; Ong, S. P.; Hautier, G.; Chen, W.; Richards, W. D.; Dacek, S.; Cholia, S.; Gunter, D.; Skinner, D.; Ceder, G.; Persson, K. A. Commentary: The Materials Project: A Materials Genome Approach to Accelerating Materials Innovation. *APL Mater.* **2013**, *1*, 011002.
(24) Ong, S. P.; Richards, W. D.; Jain, A.; Hautier, G.; Kocher, M.; Cholia, S.; Gunter, D.; Chevrier, V. L.; Persson, K. A.; Ceder, G. Python Materials Genomics (Pymatgen): A Robust, Open-Source Python Library for Materials Analysis. *Comput. Mater. Sci.* **2013**, *68*, 314−319.
(25) Hautier, G.; Fischer, C.; Ehrlacher, V.; Jain, A.; Ceder, G. Data Mined Ionic Substitutions for the Discovery of New Compounds. *Inorg. Chem.* **2011**, *50*, 656−663.
(26) Bergerhoff, G.; Hundt, R.; Sievers, R.; Brown, I. D. The Inorganic Crystal Structure Data Base. *J. Chem. Inf. Model.* **1983**, *23* (2), 66−69.
(27) Kempa, P. B.; Wiebcke, M.; Felsche, J. Structure of Trisodium Monothioarsenate Dodecahydrate. *Acta Crystallogr., Sect. C: Cryst. Struct. Commun.* **1990**, *46*, 729−732.
(28) Goldstein, B. M. Disorder in the Structure of Trisodium Phosphorothioate Dodecahydrate. *Acta Crystallogr., Sect. B: Struct. Crystallogr. Cryst. Chem.* **1982**, *38*, 1116−1120.
(29) Hermann, A.; Schwerdtfeger, P. Blueshifting the Onset of Optical UV Absorption for Water under Pressure. *Phys. Rev. Lett.* **2011**, *106*, 187403.
(30) Cockcroft, J. K.; Fitch, A. N. The Solid Phases of Deuterium Sulphide by Powder Neutron Diffraction. *Z. Kristallogr.* **1990**, *193*, 1−19.
(31) Aykol, M.; Kim, S.; Hegde, V. I.; Snydacker, D.; Lu, Z.; Hao, S.; Kirklin, S.; Morgan, D.; Wolverton, C. High-Throughput Computational Design of Cathode Coatings for Li-Ion Batteries. *Nat. Commun.* **2016**, *7*, 13779.
(32) Radhakrishnan, B.; Ong, S. P. Aqueous Stability of Alkali Superionic Conductors from First-Principles Calculations. *Front. Energy Res.* **2016**, *4*, 16.
(33) Persson, K. A.; Waldwick, B.; Lazic, P.; Ceder, G. Prediction of Solid-Aqueous Equilibria: Scheme to Combine First-Principles Calculations of Solids with Experimental Aqueous States. *Phys. Rev. B: Condens. Matter Mater. Phys.* **2012**, *85*, 235438.
(34) Kresse, G.; Furthmuller, J. Efficient Iterative Schemes for Ab Initio Total-Energy Calculations Using a Plane-Wave Basis Set. *Phys. Rev. B: Condens. Matter Mater. Phys.* **1996**, *54*, 11169.
(35) Kresse, G.; Furthmüller, J. Efficiency of Ab-Initio Total Energy Calculations for Metals and Semiconductors Using a Plane-Wave Basis Set. *Comput. Mater. Sci.* **1996**, *6*, 15−50.
(36) Kresse, G.; Joubert, D. From Ultrasoft Pseudopotentials to the Projector Augmented-Wave Method. *Phys. Rev. B: Condens. Matter Mater. Phys.* **1999**, *59*, 1758−1775.
(37) Shang, S. L.; Wang, Y.; Guan, P. W.; Wang, W. Y.; Fang, H. Z.; Anderson, T.; Liu, Z.-K. Insight into Structural, Elastic, Phonon, and Thermodynamic Properties of α-Sulfur and Energy-Related Sulfides: A Comprehensive First-Principles Study. *J. Mater. Chem. A* **2015**, *3*, 8002−8014.
(38) Perdew, J. P.; Burke, K.; Ernzerhof, M. Generalized Gradient Approximation Made Simple. *Phys. Rev. Lett.* **1996**, *77* (18), 3865−3868.
(39) Perdew, J. P.; Ruzsinszky, A.; Csonka, G. I.; Vydrov, O. A.; Scuseria, G. E.; Constantin, L. A.; Zhou, X.; Burke, K. Restoring the Density-Gradient Expansion for Exchange in Solids and Surfaces. *Phys. Rev. Lett.* **2008**, *100*, 136406.
(40) Grimme, S.; Antony, J.; Ehrlich, S.; Krieg, H. A Consistent and Accurate Ab Initio Parametrization of Density Functional Dispersion Correction (DFT-D) for the 94 Elements H-Pu. *J. Chem. Phys.* **2010**, *132*, 154104.
(41) Wang, Y.; Wang, J. J.; Wang, W. Y.; Mei, Z. G.; Shang, S. L.; Chen, L. Q.; Liu, Z. K. A Mixed-Space Approach to First-Principles Calculations of Phonon Frequencies for Polar Materials. *J. Phys.: Condens. Matter* **2010**, *22*, 202201.
(42) Wang, Y.; Chen, L.-Q.; Liu, Z.-K. YPHON: A Package for Calculating Phonons of Polar Materials. *Comput. Phys. Commun.* **2014**, *185*, 2950−2968.
(43) Wang, Y.; Shang, S.-L.; Fang, H.; Liu, Z.-K.; Chen, L.-Q. First-Principles Calculations of Lattice Dynamics and Thermal Properties of Polar Solids. *npj Comput. Mater.* **2016**, *2*, 16006.
(44) Wang, Y.; Liu, Z. K.; Chen, L. Q. Thermodynamic Properties of Al, Ni, NiAl, and Ni_3Al from First-Principles Calculations. *Acta Mater.* **2004**, *52*, 2665−2671.

DOI: 10.1021/acsami.7b03606
ACS Appl. Mater. Interfaces 2017, 9, 16261−16269

(45) Shang, S. L.; Wang, Y.; Kim, D.; Liu, Z. K. First-Principles Thermodynamics from Phonon and Debye Model: Application to Ni and Ni_3Al. *Comput. Mater. Sci.* **2010**, *47*, 1040−1048.
(46) Shang, S. L.; Saengdeejing, A.; Mei, Z. G.; Kim, D. E.; Zhang, H.; Ganeshan, S.; Wang, Y.; Liu, Z. K. First-Principles Calculations of Pure Elements: Equations of State and Elastic Stiffness Constants. *Comput. Mater. Sci.* **2010**, *48*, 813−826.
(47) Shang, S.-L.; Zhou, B.-C.; Wang, W. Y.; Ross, A. J.; Liu, X. L.; Hu, Y.-J.; Fang, H.-Z.; Wang, Y.; Liu, Z.-K. A Comprehensive First-Principles Study of Pure Elements: Vacancy Formation and Migration Energies and Self-Diffusion Coefficients. *Acta Mater.* **2016**, *109*, 128−141.
(48) Gammon, P. H.; Kiefte, H.; Clouter, M. J. Elastic Constants of Ice Samples by Brillouin Spectroscopy. *J. Phys. Chem.* **1983**, *87*, 4025−4029.
(49) Sasaki, S.; Shimizu, H. High-Pressure Brillouin Study on Orientationally Disordered Solid Phase I of H_2S and D_2S. *J. Phys. Soc. Jpn.* **1995**, *64*, 3309−3314.
(50) Shimizu, H.; Sasaki, S. High-Pressure Brillouin Studies and Elastic Properties of Single-Crystal H_2S Grown in a Diamond Cell. *Science* **1992**, *257*, 514−516.
(51) Bischoff, C.; Schuller, K.; Haynes, M.; Martin, S. W. Structural Investigations of $yNa_2S + (1-y)PS_{5/2}$ Glasses Using Raman and Infrared Spectroscopies. *J. Non-Cryst. Solids* **2012**, *358*, 3216−3222.
(52) Blachnik, R.; Rabe, U. Das Thermische Verhalten Der Mischungen Na_2S-P_4S_{10} und $Na_4Ge_4S_{10}$-P_4S_{10} des Systems Na_2S-GeS_2-P_4S_{10}. *Z. Anorg. Allg. Chem.* **1980**, *462*, 199−206.
(53) Kopylov, N. I.; Minkevich, S. M. The As_2S_3-Na_2S System. *Russ. J. Inorg. Chem.* **1975**, *20*, 1744−1746.
(54) Heyd, J.; Scuseria, G. E.; Ernzerhof, M. Hybrid Functionals Based on a Screened Coulomb Potential (Vol. 118, P. 8207, 2003). *J. Chem. Phys.* **2006**, *124*, 219906.
(55) Mereiter, K.; Preisinger, A.; Zellner, A.; Mikenda, W.; Steidl, H. Hydrogen-Bonds in α-$Na_3PS_4 \cdot 8H_2O$ - X-Ray Diffraction and Vibrational Spectroscopic Study. *Inorg. Chim. Acta* **1983**, *72*, 67−73.
(56) Pompetzki, M.; Jansen, M. Crystal Structures of $Na_3PO_2S_2 \cdot 11H_2O$ and $Na_3POS_3 \cdot 11H_2O$. *Monatsh. Chem.* **2002**, *133*, 975−986.
(57) Pompetzki, M.; Dinnebier, R. E.; Jansen, M. Sodium dithiophosphate (V): Crystal Structure, Sodium Ionic Conductivity and Dismutation. *Solid State Sci.* **2003**, *5*, 1439−1444.
(58) Pompetzki, M.; Jansen, M. Sodium Trithiophosphate (V): Crystal Structure and Sodium Ionic Conductivity. *Z. Anorg. Allg. Chem.* **2003**, *629*, 1929−1933.
(59) Pompetzki, M.; Jansen, M. Sodium Monothiophosphate (V): Crystal Structure and Sodium Ionic Conductivity. *Z. Anorg. Allg. Chem.* **2002**, *628*, 641−646.
(60) Chemiday. http://chemiday.com/en/reaction/3-1-0-9559 (accessed Nov 1, 2016).
(61) Luo, Y.-R. *Comprehensive Handbook of Chemical Bond Energies*; CRC Press: Boca Raton, FL, 2007.

DOI: 10.1021/acsami.7b03606
ACS Appl. Mater. Interfaces 2017, 9, 16261−16269